Received 17 April 2023; revised 23 May 2023; accepted 3 June 2023. Date of publication 7 June 2023; date of current version 21 June 2023.
The review of this article was arranged by Editor Z. Zhang.

Digital Object Identifier 10.1109/JEDS.2023.3283533

Design and Fabrication of PDMS Microfluidic Device Combined With Urea Biosensor for Dynamic and Static Measurements

PO-YU KUO (Member, IEEE), TAI-HUI WANG (Student Member, IEEE), MING-TAI HSU, AND CHI-HAN LIAO

Graduate School of Electronic Engineering, National Yunlin University of Science and Technology, Douliou 64002, Taiwan

CORRESPONDING AUTHOR: P.-Y. KUO (e-mail: kuopy@yuntech.edu.tw)

This work was supported by the National Science and Technology Council, Taiwan, under Grant NSTC 111-2221-E-224-050 and Grant NSTC 111-2221-E-224-058.

ABSTRACT In this study, a more efficient, convenient, and cost-effective way was proposed to design and fabricate a polydimethylsiloxane (PDMS) microfluidic device using 3D printing and transfer techniques. Typically, sensor measurements can only be conducted by immersing the sensor in a solution under static conditions. However, in this study, a newly designed microfluidic device combined with a microfluidic system enables dynamic measurements with sensors. By controlling the flow and temperature of the test liquid, the physiological environment of the human body under various conditions can be simulated, resulting in more accurate and realistic data. During the dynamic condition, an average sensitivity of 6.396 mV/(mg/dL) and linearity of 0.999 were obtained at a flow rate of 75.0 μL/min. When the temperature was at 37°C, the biosensor achieved an average sensitivity of 4.381 mV/(mg/dL) and a linearity of 0.999. The dynamic response time was 7 seconds, and the drift rate was 1.47 mV/hr. The experimental results obtained under dynamic conditions showed a significant improvement in the sensing characteristics of the urea biosensor compared with the results obtained under static conditions.

INDEX TERMS Static measurement, dynamic measurement, PDMS, microfluidic, urea biosensor.

I. INTRODUCTION

UREA is a relatively simple compound that is composed of two amino groups and a carbon atom. It is produced in the liver through a process called the urea cycle, which involves the conversion of excess amino acids into urea. Urea is then excreted in the urine, along with other waste products of protein metabolism. The concentration of urea in urine is an important indicator of kidney function, as the kidneys are responsible for filtering and eliminating waste products from the body. An abnormal concentration of urea in the urine can be a sign of kidney disease or other conditions that affect the kidneys [1]. For example, high levels of urea in the urine may be a sign of kidney damage or reduced kidney function, while low levels of urea may be a sign of malnutrition or other conditions that affect protein metabolism [2]. The concentration of urea in urine can also be affected by factors such as diet, fluid intake, and medication use, and may be influenced by other factors such as age and overall health status. Urea is an important biomarker that is often used in conjunction with other tests to diagnose and monitor kidney disease and other conditions that affect the kidneys [3], [4], [5].

An electrochemical biosensor is a device that uses biological materials as the sensing element for biosensing [6], [7]. Electrochemical biosensors can be used for a variety of applications, including medical diagnostics [8], [9], food safety testing [10], [11], environmental monitoring [12], [13], and bioanalysis [14]. For example, they can be used to detect urea levels in the blood, toxins or viruses in water, and harmful substances in the air. Electrochemical biosensors have many advantages, including high accuracy, fast detection speed, and low cost.

Microfluidic devices have a wide range of applications, including medical diagnostics, drug delivery, chemical synthesis, and environmental monitoring [14]. The integration of microfluidics with biosensors allows for the precise

control and manipulation of small volumes of fluids in combination with the detection of specific biomolecules [15], [16], [17], [18]. Microfluidic systems can be used to simulate the human body environment, including flow rate, pH, and temperature under physiological conditions. The advantage of dynamic measurement using microfluidic systems is that electrochemical measurements can be performed with a very small amount of solution. By precisely controlling the flow rate of the liquid through the microfluidic system to simulate the complex blood flow environment inside the human body, it can be used to study changes in blood flow rate and urea concentration to determine the physiological status of the human body. This provides the possibility for future implantation of sensing chips in the human body. The use of this measurement method for real-time monitoring can achieve advantages such as reducing measurement costs and enabling rapid analysis.

Soft lithography is currently the mainstream technology for manufacturing microfluidic devices [19], [20], [21] However, the production process is complex and time-consuming, requiring multiple steps and specialized equipment. This increases the cost and time required to manufacture microfluidic devices using this technology. We propose a fast, convenient, and low-cost method for producing fluidic devices using 3D printing technology.

3D printing is a machine that creates physical objects by depositing materials layer by layer based on a digital model [22], [23]. The technology has been applied in the field of microfluidics to manufacture complex and intricate microfluidic devices that are difficult or impossible to produce using traditional manufacturing techniques [24], [25], [26]. In this work, we propose a 3D printing and transfer method for fabricating microfluidic devices that consumes less time and cost than traditional soft lithography methods. Additionally, we combine the microfluidic device with a urea biosensor based on a urease/RuO_2/silver/PET sensing membrane for dynamic and static measurements.

In previous research, our research group designed an instrumentation amplifier readout circuit using cross-coupling techniques [27]. This readout circuit can output small signals with high precision, making it an ideal choice for measuring the sensitivity of a biosensor. In this study, we applied this readout circuit in a V-T measurement system to measure the sensing characteristics of the biosensor. By using this system, we can accurately and reproducibly measure the signals of the biosensor over a wide range of analyte concentrations.

II. EXPERIMENT PROCEDURE

This section is presented in four parts: the first part presented the materials used; the second part Fabrication of the arrayed urease/RuO_2 sensing windows and the silver reference electrodes; the third part designed and manufactured the microfluidic device model and the microfluidic channel model; the fourth part manufactured the microfluidic device.

A. MATERIALS

The polyethylene terephthalate (PET) substrate was bought from Zencatec Corporation (Tao-Yuan City, Taiwan), the RuO_2 target (99.95% purity) from Ultimate Materials Technology Co., Ltd (Hsinchu County, Taiwan), the silver paste from Advanced Electronic Material Inc. (Tainan City, Taiwan), the epoxy thermosetting polymer from Sil-More Industrial, Ltd. (New Taipei City, Taiwan), the urease was purchased from Sigma-Aldrich Corp. (St. Louis, Missouri, USA), the Urea powder was purchased from J. T. Baker Corp. (St. Louis, MO, USA), the 3-Aminopropyltriethoxysilane (γ-APTES), and the glutaraldehyde was from Sigma-Aldrich Corp, (St. Louis, MO, USA). The pH 7.0 phosphate-buffered saline (PBS) was purchased from AppliChem GmbH Crop. (Darmstadt, Germany), which was used to prepare different concentrations of urea solutions and prepared specific ratios of γ-APTES, glutaraldehyde, and urease solutions. The SYLGARD 184 A-B Silicone elastomer kit (PDMS) was bought from UniRegion Bio-Tech Co., Ltd (Hsinchu, Taiwan).

B. FABRICATION OF THE ARRAYED UREASE/RUO2 SENSING WINDOWS AND THE SILVER REFERENCE ELECTRODES

In this study, we prepared a urease/RuO_2 biosensor based on the methods described in Chou's research [28] and the structure formulations previously reported [27]. To fabricate the RuO_2 membrane, we have developed a biosensor based on a 30 mm $\times$ 40 mm PET substrate. At first, we used the screen printing technique to make the silver paste on the PET substrate to manufacture six sensing windows and two reference electrodes based on the PET substrate. Then, the radio frequency (RF) sputtering system was used to deposit the RuO_2 thin film on the silver wire / PET substrate by the RuO_2 target at the power of 50 W, 20 mTorr of deposition pressure, 10 sccm of argon gas flow, and 1 sccm of oxygen gas flow for 30 minutes. We have summarized the sputtering parameters in Table 1. The screen printing technique was used to cover the epoxy resin on the silver wire and avoid the six sensing windows and two reference electrodes to prevent the silver wire eroded by the urea solution. The γ-APTES (99 wt%) solution of 2 μL was dropped on the RuO_2 thin film and 2 μL of the glutaraldehyde solution (1 wt%) was dropped onto the γ-APTES film Then, 2 μL of urease crosslinker solution was dropped on the glutaraldehyde film. Finally, we store it at 4°C for 24 hours to stabilize its structure [29], [30] The structure of the arrayed RuO_2 urea biosensor was shown in Figure 1. The RuO_2 layer, serving as the ion sensing film, is combined with the working electrode. Due to its excellent electrochemical characteristics, stability, and good biocompatibility, it can enhance the sensitivity and signal-to-noise ratio of the ion sensor. When the test solution comes into contact with the sensing film, it is used to convert the sensed biochemical information into an electrical signal. The surface morphology of the sensor layer was analyzed by a field emission scanning electron microscope (FE-SEM)

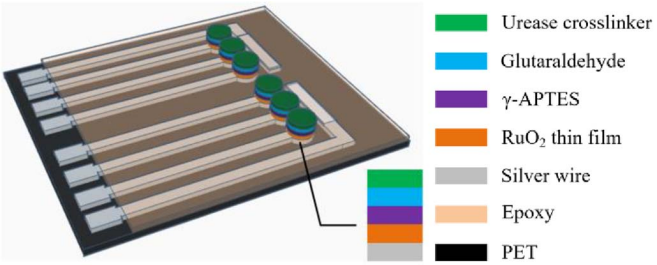

FIGURE 1. The structure diagram of the arrayed urea biosensor.

TABLE 1. The parameters for the RuO_2 thin film.

Target	RuO_2
RF Power (W)	50
Deposition Pressure (mTorr)	20
Gas Flow (Ar: O_2, sccm)	10:1
Deposition Time (min)	30

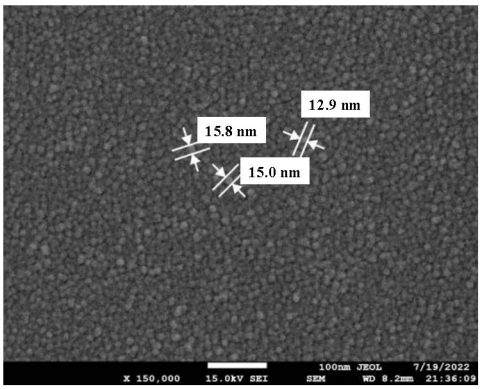

FIGURE 2. The top view surface analysis of the RuO_2 sensing layer.

and shown in Figure 2, with an average grain size between 12.9 nm and 15.8 nm.

C. DESIGN AND MANUFACTURE OF THE MICROFLUIDIC DEVICE MODEL AND MICROFLUIDIC CHANNEL MODEL

Firstly, we used 3D drawing software to design the fluid channel of the target microfluidic devices. The length and width of the fluid channel were chosen based on the dimensions of blood vessels in the human body and the flow limitations of microfluidic systems. The structure was designed based on the position of six sensing windows and two reference electrodes. After completing the 3D modeling of the microfluidic channel, a microfluidic model was designed. A flat surface and a fixed border were added to facilitate its fabrication. The size of the whole 3D microfluidic model is 40 mm × 40 mm × 20 mm. Figure 3(a) shows the 3D microfluidic device model and (b) shows the 3D microfluidic channel model.

We used a 3D printer to produce the 3D microfluidic device model and the 3D microfluidic channel model that we designed, using polylactide (PLA) as the material [31] With the help of 3D printing, we were able to quickly

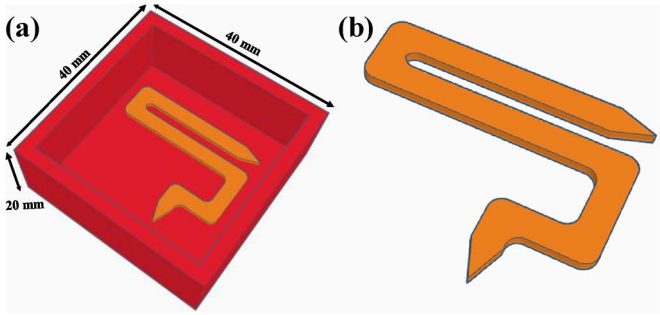

FIGURE 3. The schematic diagram of (a) the 3D microfluidic device model and (b) the 3D microfluidic channel model.

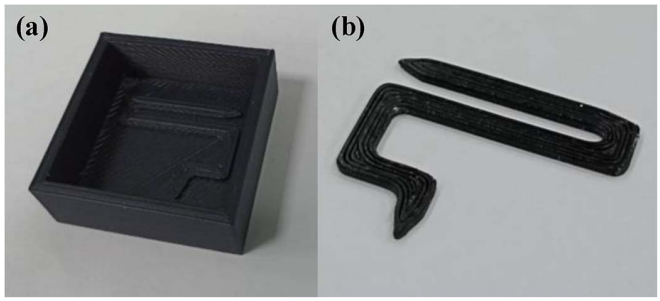

FIGURE 4. The entity diagram of (a) the microfluidic device model and (b) the microfluidic channel model.

fabricate a functional prototype of our microfluidic device, which allowed us to test and optimize the performance of our device before mass production. This approach greatly improves the efficiency and accuracy of the fabrication process. Furthermore, the use of PLA as the material also provides an advantage in terms of biocompatibility and stability. Figure 4(a) shows the entity diagram of the microfluidic device model and Figure 4(b) shows the entity diagram of the microfluidic channel model.

The microfluidic device was made by using the model shown in Figure 4. We prepared a polydimethylsiloxane (PDMS) solution by mixing SYLGARD 184 A-B in a 10:1 ratio. The mixture was stirred until homogenous. Next, we degassed the mixture to remove any bubbles that formed during mixing. Finally, we poured the prepared PDMS solution into the model shown in Figure 4(a), taking into account the heat resistance of the 3D printing material and the characteristics of PDMS. We baked the microfluidic model with PDMS solution in the ovens at 70 °C for one hour. Then, the microfluidic device was removed from the microfluidic model and baked in an oven again at 120 °C for one hour to harden it. The microfluidic device made in this experiment was shown in Figure 4(a) and the size is 35mm×35mm×15mm, the width of the channel is 2.5 mm, and the depth is 0.5 mm. However, due to the use of a 3D printed model for transfer printing, the surface of the microfluidic device is uneven, which prevents it from forming a tight seal with the sensor. In this study, we proposed a solution to this problem. We used the channel model shown

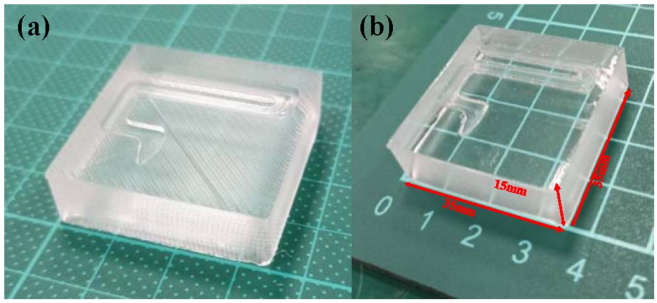

FIGURE 5. The entity diagram of (a) the microfluidic device before modification and (b) the microfluidic device after modification.

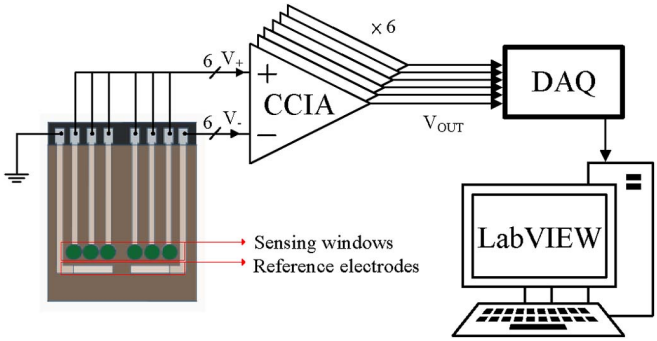

FIGURE 6. The schematic diagram of the V-T measurement system combined with the arrayed urease/RuO_2 urea biosensor.

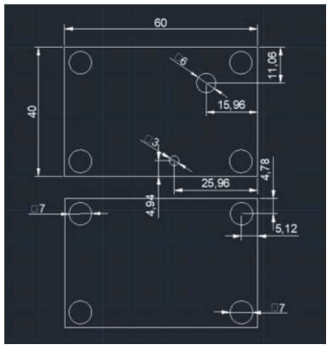

FIGURE 7. The schematic diagram of the PMMA board model.

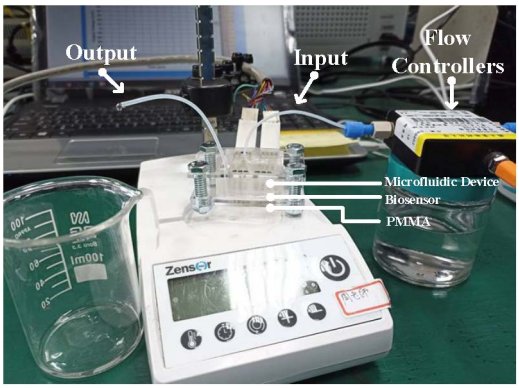

FIGURE 8. The entity diagram of the microfluidic device combination with the urea biosensor.

in Figure 4(b) and placed it inside the microfluidic device shown in Figure 4(a). We then used a spin coating method, with the parameters set at 1500 rpm for 30 seconds, to evenly coat the surface of the microfluidic device with the PDMS solution. After that, we removed the channel model and baked the microfluidic device at 120 °C for one hour to cure the PDMS on its surface. The modified microfluidic device is shown in Figure 5(b).

D. THE DYNAMIC MEASUREMENT SYSTEM

A dynamic measurement system can be composed of a V-T measurement system and a microfluidic measurement system. The V-T measurement system is a circuit that can measure the voltage and time response of a biosensor, while the microfluidic measurement system is a device that can control and manipulate the flow of fluids, such as the samples and reagents, to the biosensor together, the V-T measurement system and microfluidic measurement system can work in concert to enable real-time, dynamic monitoring of the response of the biosensor over time, as the biosensor interacts with target molecules or analytes in a controlled fluidic environment.

Figure 6 shows the schematic diagram of the V-T measurement system combined with the arrayed urease/RuO_2 urea biosensor. The cross-coupled instrumentation amplifier (CCIA), which is a biomedical signal readout circuit proposed in previous research [27], has the characteristics of a high common-mode rejection ratio (CMRR) and low unity gain frequency (UGF) and is well-suited for measuring biomedical signals. The output voltage of CCIA (V_{OUT}) is given by:

$$V_{OUT} = V_+ - V_- \tag{1}$$

We integrated the microfluidic device produced in this experiment with the urea biosensor. To consider the repeated use of the device for laboratory testing, the poly methyl methacrylate (PMMA) upper and lower covers were designed as shown in Figure 7. It contains four corner fixing holes and liquid inflow and outflow retention holes, the overall size is 60 mm × 40 mm, which is used to fix the urea sensor and microfluidic device as shown in Figure 8. The device can achieve the effect of repeated use by simply replacing the urea biosensor. Figure 9 shows the entity diagram of the dynamic measurement system. The dynamic measurement system is made up of a V-T measurement system and a microfluidic system. The V-T measurement system includes (a) CCIA readout circuit chips, (b) a power supply that provides driving voltage, (c) a data acquisition device (DAQ, USB-6210 from the National Instruments Corp., Austin, TX, USA) for transmitting biological signals, and (d) LABVIEW software. The microfluidic system includes (e) a microfluidic control system (OB1 MK3$^+$ from Elvesys Microfluidic Innovation Center, France) that uses nitrogen as a pressure source to drive the solution in the

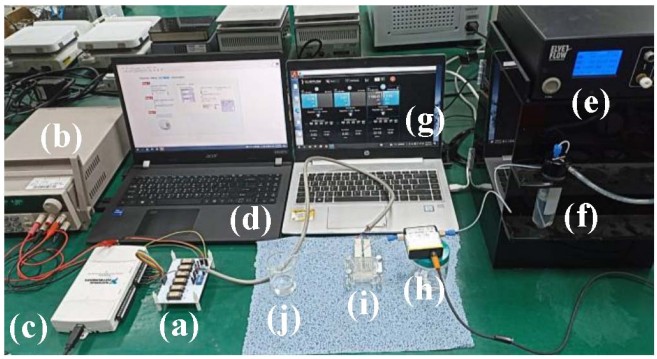

FIGURE 9. The entity diagram of the dynamic measurement system.

TABLE 2. The comparisons of the stability of silver reference electrode.

Number of samples	Urea concentration (mg/dL)	electric potential (mV)	standard deviation (mV)	RSD (%)
60	10	35.3752	0.1997	0.56
	20	35.9915	0.2074	0.58
	30	35.6153	0.2112	0.59
	40	36.1171	0.2404	0.67
	50	35.7544	0.2252	0.63

(f) a test tube, (g) microfluidic control software and (h) a flow controller to control the flow of liquid, allowing the test liquid to enter (i) the urea biosensor through the channel on the microfluidic device and complete the electrochemical reaction. The waste liquid then flows from the iron fluorine dragon tube into (j) a beaker.

III. RESULTS AND DISCUSSION

In this section, the discussions of static and dynamic measurement systems were used to analyze the sensing characteristics of the prepared urea biosensor.

A. THE STABILITY OF THE SILVER REFERENCE ELECTRODE

Ag demonstrates potential as a reference electrode due to its chemical stability [32]. Chou et al. [28] developed a biosensor and replaced the conventional bulky Ag/AgCl reference electrode with a silver reference electrode. We conducted stability tests on the silver electrode using a V-T measurement system, measuring the voltage potential between the silver reference electrode and the ground. By immersing the silver electrode in urea solutions of varying concentrations, we recorded the response voltage to the ground and calculated the relative standard deviation to assess its stability. The measurement data was consolidated in Table 2, and the obtained relative standard deviations were all below 1%. Based on the measurement results, we can conclude that the silver reference electrode demonstrates excellent stability.

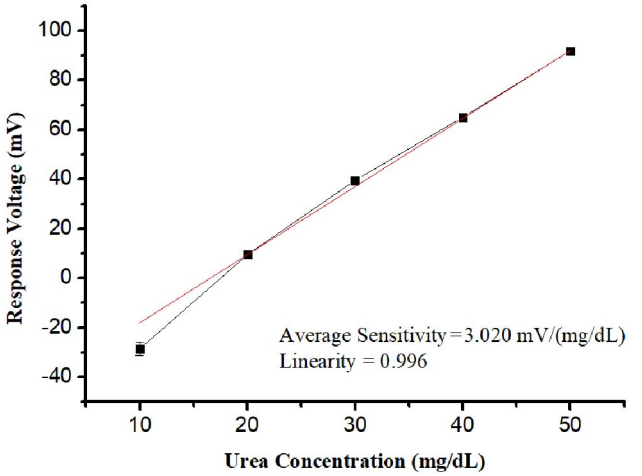

FIGURE 10. The average sensitivity and the linearity of the urea biosensor were measured by the static measurement system.

B. AVERAGE SENSITIVITY AND THE LINEARITY OF UREA BIOSENSOR

To mimic the concentration of urea in the human body [33], we prepared different urea solutions with five concentrations of 10 mg/dL, 20 mg/dL, 30 mg/dL, 40 mg/dL, and 50 mg/dL, respectively. We used a voltage-time (V-T) measurement system in static measurement and immersed the urea biosensor in the solutions with the above concentrations. In static measurement, the average sensitivity and the linearity of the urea biosensor are shown in Figure 10. The average sensitivity of the urea biosensor was 3.020 mV/(mg/dL), and the linearity was 0.996. The formula of average sensitivity is given by:

$$S = \frac{\Delta V}{R} \tag{2}$$

where

S refers to the average sensitivity of the biosensor

ΔV refers to the voltage signal change of the biosensor

R refers to the concentration range of the test solution.

In dynamic measurement, we used a microfluidic system to control the fluid velocity to flush the urea biosensor with the above concentration of fluid [34], [35]. In the human microvasculature, the flow velocity of blood ranges between 0.3 mm/s and 1 mm/s depending on its motion state [36], [37] Through the microfluidic system, we control the flow rate of the solution (μL/min) and simulate different solution flow rates under different conditions using the microfluidic device. The sensing characteristics of the urea biosensor are recorded and analyzed under different flow rates. The conversion between liquid flow rate and flow velocity can be calculated using the formula given by:

$$Q = A \times V \tag{3}$$

where

Q refers to the flow rate of the solution, and the unit is microliters per minute (μL/min)

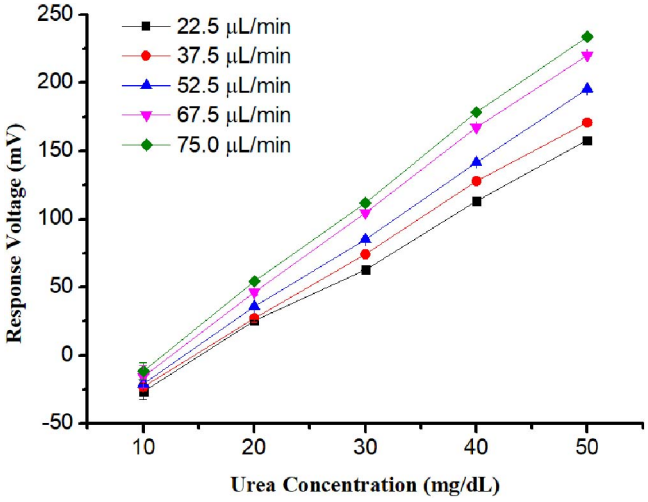

FIGURE 11. The average sensitivity and the linearity of the urea biosensor were measured by the dynamic measurement system.

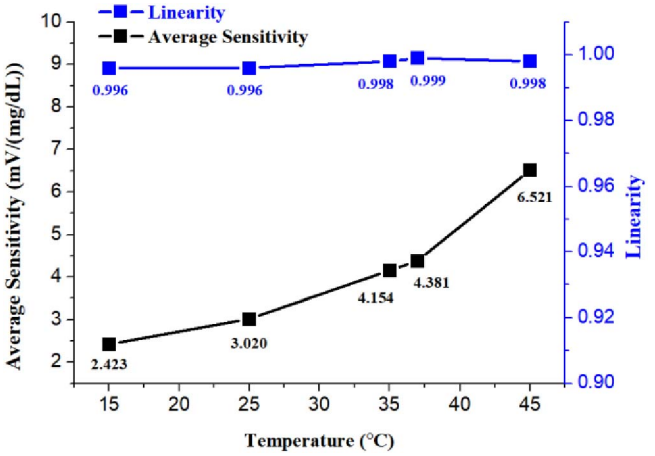

FIGURE 12. The temperature effect of the urea biosensor in 10 mg/dL to 50 mg/dL at 15C to 45C.

A refers to the cross-sectional area of the microfluidic channel, and its unit is typically square millimeters (mm^2)

V refers to the flow velocity of the solution, with units of millimeters per second (mm/s).

According to the calculation, the corresponding flow rate for the velocity of 0.3 mm/s in this experiment is 22.5 μL/min, while the corresponding flow rate for the velocity of 1 mm/s is 75 μL/min. In dynamic measurement, we selected 22.5 μL/min, 37.5 μL/min, 52.5 μL/min, 67.5 μL/min, and 75.0 μL/min as the flow rates to measure the average sensitivity and linearity of the urea biosensor under dynamic conditions. The measurement results are shown in Figure 11. The results are also consolidated in Table 3. The measurement results show that the sensing characteristics of the urea biosensor under dynamic conditions are superior to that under static conditions, and the urea sensor's average sensitivity increases as the solution's flow rate increases. This phenomenon is attributed to the variation in the catalytic rate of the urease enzyme and the diffusion resistance of the sensing membrane in a dynamic environment [38], [39], where the liquid flows through the sensing window of the sensor at different flow rates in the microfluidic system. The reactants are transmitted to the interior of the sensing membrane through diffusion. The diffusion efficiency is influenced by the diffusion resistance of the membrane, which can be reduced by increasing the flow rate. As the flow rate increases, the diffusion resistance of the sensing membrane decreases.

The average sensitivity and linearity of the urea sensor at a flow rate of 22.5 μL/min are 4.552 mV/(mg/dL) and 0.997, respectively. At a flow rate of 37.5 μL/min, they are 4.802 mV/(mg/dL) and 0.998, respectively. At a 52.5 μL/min flow rate, they are 5.401 mV/(mg/dL) and 0.998, respectively. At a flow rate of 67.5 μL/min, they are 6.191 mV/(mg/dL) and 0.999, respectively. At a 75.0 μL/min flow rate, they are 6.396 mV/(mg/dL) and 0.999, respectively. Compared to static measurements, the dynamic measurements in this experiment showed an increase in the average sensitivity of the urea sensor of 50.7% to 111.8% based on its flow rate.

C. TEMPERATURE EFFECT OF UREA BIOSENSOR

The temperature effect experiment of the urea biosensor. This experiment uses a constant temperature water bath (FIRSTEK MODEL-8402L) to raise or lower the temperature of the urea solution to a specified temperature and measure the average sensitivity and linearity of the biosensor at the specified temperature. The tested in this experiment. The temperature is 15°C below room temperature, 25°C room temperature, 35°C close to normal body temperature, 37°C above normal body temperature, and 45°C higher than normal body temperature. The main purpose of this experiment In order to measure and analyze the change of the average sensitivity and linearity of the biosensor with the change of temperature and to simulate the performance of the sensing characteristics of the biosensor under the normal body temperature of the human body; the measurement results are shown in Figure 12. In general, the average sensitivity and the linearity experiments of the biosensor are carried out at room temperature with a solution temperature of 25 °C. This experiment mainly simulates the biosensor's performance at the normal temperature of the human body. We use the V-T measurement system to measure. The urea biosensor is used to measure the average sensitivity and the linearity.

The average sensitivity is 2.423 (mV/(mg/dL)), and the linearity is 0.996 when the solution temperature is 15 °C. When the solution temperature is 25 °C, the average sensitivity is 3.020 (mV/(mg/dL)), and the linearity is 0.996. As the temperature of the solution rises, the average sensitivity of the urea biosensor also increases. When the solution temperature reaches 35 °C, the urea biosensor's measured average sensitivity is 4.154 (mV/(mg/dL)), and the linearity is 0.998. When the solution temperature reaches 37 °C, the measured average sensitivity of the urea biosensor is 4.381 (mV/(mg/dL)) linearity is 0.999, and its average

TABLE 3. The comparisons of the average sensitivity and the linearity of urea biosensors.

Sensing Membrane	Flow Velocity (mm/s)	Flow Rate (μL/min)	Liner Range (mg/dL)	Average Sensitivity mV/(mg/dL)	Linearity
Urease(6:4) / RuO_2	0	0	10-50	3.020	0.996
	0.3	22.5		4.552	0.997
	0.5	37.5		4.802	0.998
	0.7	52.5		5.401	0.998
	0.9	67.5		6.191	0.999
	1.0	75.0		6.396	0.999

sensitivity is increased by 45.1% compared with the solution at room temperature. When the solution temperature rises to 45 °C again, the measured average sensitivity of the urea biosensor is 6.521 (mV/(mg/dL)). The linearity is 0.998, and the average sensitivity is increased by 115.9% compared with the solution at room temperature. As the temperature increases, the sensing characteristics of the urea biosensor also increase. We attribute it to the increase in urease activity when the temperature increases. According to the research by Barbara et al., the optimal activity of urease occurs at 65 °C [40].

D. RESPONSE TIME OF UREA BIOSENSOR

Response time is also one of the important sensing properties of a biosensor. Firstly, we conducted an experiment on response time under static conditions. We used a V-T measuring system to measure the biosensor and immersed the biosensor in 50 mL PBS solution. After the reaction stabilized, we dropped 250 μL of 30mg/dL urea solution at 30 seconds and observed the response voltage change. The formula for response time is given as follows [41]:

$$T_{RT} = T_{V_{95}-T_{V_0}} \tag{4}$$

$$V_{95} = V_0 + (V_F - V_0) \times 95\% \tag{5}$$

where

T_{RT} refers to the response time of the biosensor

$T_{V_{95}}$ refers to the time point at which the biosensor completes 95% of the response.

T_{V_0} refers to the time point at which the sensor becomes stable in PBS solution and starts to respond

V_{95} refers to the 95% of the steady-state response voltage reached from V_0

V_0 refers to the response voltage value of the biosensor when it is stable in PBS solution.

V_F refers to the highest response voltage value of the biosensor after reaction with the analyte.

The results of response time under static conditions are shown in Figure 13. The biosensor was stable at a response voltage of −73.00 mV at 30 seconds. After the urea solution was dropped, the voltage could reach −69.32 mV. Response time is the time required from the initial voltage to reach 95% of the steady-state voltage. According to the formula (4) and formula (5), the calculated response time was 11 seconds.

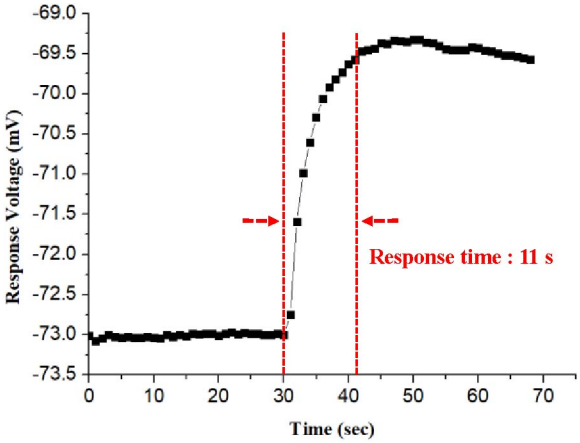

FIGURE 13. The response time of the urea biosensor under static condition.

For the experiment on response time under dynamic conditions, we used a dynamic measuring system. We combined the biosensor with a microfluidic device and used PBS buffer solution to continuously inject the solution into the microfluidic device at a flow rate of 22.5 μL/min. After the reaction stabilized, we injected 7.5 μL of 30mg/dL urea solution at 30 seconds using a syringe and observed the change in response voltage, as shown in Figure 14. The biosensor was stable at a response voltage of −65.66 mV at 30 seconds. After the urea solution was injected, the voltage could reach −63.57 mV. Based on formula (4) and formula (5), we calculated the dynamic response time to be 7 seconds. The results are also consolidated in Table 4. We also conducted response time experiments under different concentrations and flow rates. The urea solutions represented low (10 mg/dL), medium (30 mg/dL), and high concentrations (50 mg/dL) within the normal range of human body. The flow rates corresponded to low (22.5 μL/min), medium (52.5 μL/min), and high flow (75 μL/min) in microvessels under different physical activities. The experimental results, as shown in Figure 15, indicate that as the flow rate and analyte concentration increase, the response time of the sensor also increases. Due to dilution effects during measurement, a decrease in the injected analyte concentration results in a

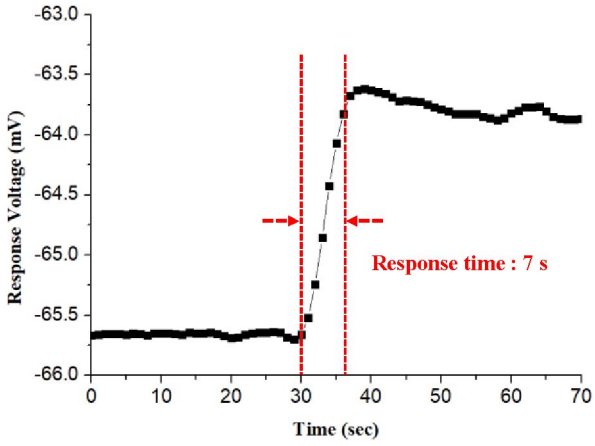

FIGURE 14. The response time of the urea biosensor under dynamic condition.

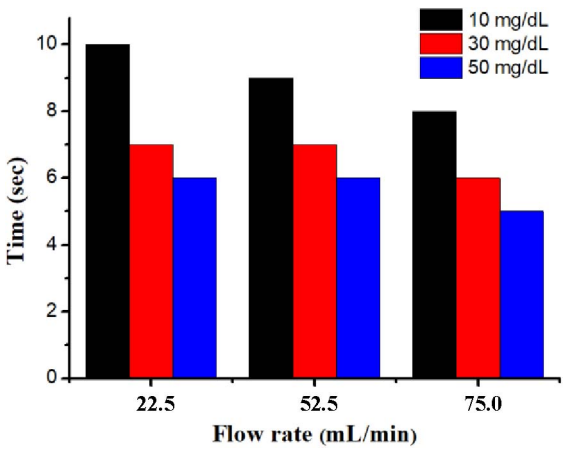

FIGURE 15. The response time of the urea biosensor under different concentrations and flow rates.

smaller change in the sensor's response voltage, leading to an increase in the response time.

E. DRIFT EFFECT OF UREA BIOSENSOR

The drift effect is an undesirable phenomenon that can compromise the accuracy of biosensors. The drift experiment is a slow-response experiment. During the long-term measurement process of the sensor in contact with the solution, a hydration layer capacitance is generated on the sensor surface, and the thickness of the hydration layer gradually increases with time. However, there is an upper limit to the thickness, and the generation of the hydration layer causes the sensor output to gradually change over time. The growth time of the hydration layer varies depending on the rate of hydration.

For measuring the static drift effect, we utilized the V-T measurement system and soaked the biosensor in a urea solution of 30 mg/dL for 12 hours and recorded its response voltage. The formula for the static drift effect is given as follows [42]:

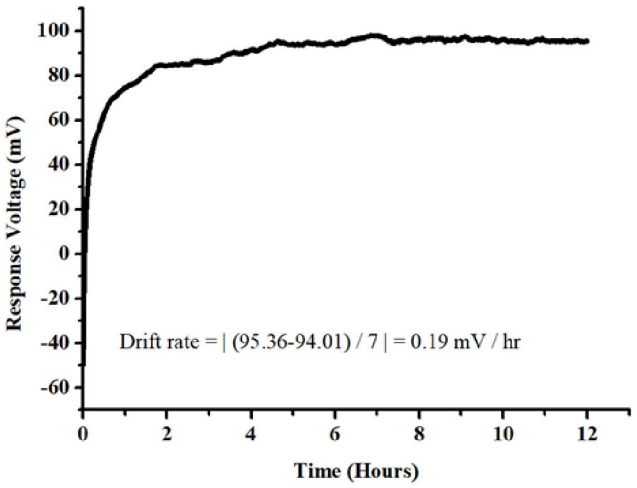

FIGURE 16. The drift effect of the urea biosensor were measured by the static measurement system.

$$V_{D\text{rift rate}} = \left| \frac{V_{D\text{rift}}}{\text{Time}} \right| = \left| \frac{V_{12^{\text{th}}\text{hr}} - V_{5^{\text{th}}\text{hr}}}{7\text{hr}} \right| \tag{6}$$

where

V_{Drift} refers to the drift voltage

$V_{(5\text{th hr})}$ refers to the response voltage of biosensor contacted to 30 mg/dL urea solution for 5th hour

$V_{(12\text{th hr})}$ refers to the response voltage of biosensor contacted to 30 mg/dL urea solution for 12th hour

As shown in Figure 16, based on the formula (6), the static drift voltage of the biosensor can be calculated by using the response voltage change over the last 7 hours of the 12 hours of data obtained from the measurement. The result shows that the static drift voltage of the biosensor is 1.35 mV, and the static drift rate of the biosensor in the same concentration of urea solution is 0.19 mV/hr.

To analyze the dynamic drift effect, we used a dynamic measurement system and infused the urea solution of 30 mg/dL at a flow rate of 22.5 μL/min (0.3 mm/s) into the microfluidic device, continuously exposing the biosensor to the solution, and recorded its response voltage for 12 hours. As shown in Figure 17, based on formula (6), the dynamic drift voltage of the urea biosensor can be calculated by using the response voltage change over the last 7 hours of the 12 hours of data obtained from the measurement. The results show that the dynamic drift voltage of the biosensor is 10.32 mV, and the dynamic drift rate of the biosensor in the same concentration of urea solution is 1.47 mV/hr. The results are also consolidated in Table 4. According to formula (6), we can calculate the average drift rate, which is lower in static conditions than in dynamic conditions. However, when observing the drift rate in different time intervals, in the static drift experiment, the values show positive and negative fluctuations in each interval, leading to mutual cancellation in the final calculation. In contrast, in the dynamic drift experiment, the values in each interval

TABLE 4. Comparisons for the sensing characteristics of the various urea biosensors.

Sensing architecture	Linear range (mg/dL)	Flow Rate (μL/min)	Sensitivity	Linearity	Response Time (seconds)	Drift Effect (mV)/hr	Ref.
Urease(6:4) / RuO_2	10-50	0	3.020 mV/(mg/dL)	0.996	11	0.19	This study
	10-50	22.5	4.552 mV/(mg/dL)	0.997	7	1.47	
Urease /GO/TiO_2	10-50	0	2.054 mV/(mg/dL)	0.979	20	7.373	2019 [43]
Urease-MBs/GO/TiO_2	10-50	0	4.966 mV/(mg/dL)	0.974	15	4.395	
Urease-MBs /GO/NiO	10-50	666.7	5.582 mV/(mg/dL)	0.959	-	-	2019 [44]
Urease-Au NPs/GO/NiO	0.03-300.3	0	52.31 mV/decade	0.998	25	-	2021 [45]
SPCE/Poly(HEMA -GMA)-Urease	0.03-1501.5	0	-	0.988	30	-	2021 [46]

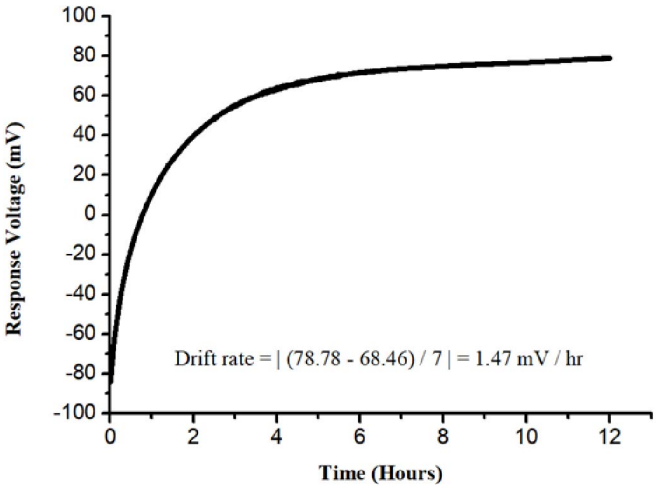

FIGURE 17. The drift effect of the urea biosensor were measured by the dynamic measurement system.

are close to the final calculation drift rate, and the overall trend shows stable positive growth. Therefore, it can be concluded that the overall trend of the biosensor under dynamic conditions is more stable.

IV. CONCLUSION

This study proposes and fabricates a PDMS microfluidic device using 3D printing and transfer printing technologies, incorporating previously designed CCIA readout circuit chips and combining them with a V-T measurement system and a microfluidic system to establish a dynamic measurement system. The aim is to simulate the physiological environment of the human body and to measure and analyze the sensing characteristics of urea biosensors. The results show that under static conditions, the urea detection has an average sensitivity of 3.020 mV/(mg/dL) and a linearity of 0.996. Under dynamic conditions, the average sensitivity and linearity of urea detection at flow rates of 0.3 mm/s and 1 mm/s are 4.552 mV/(mg/dL), 0.997 and 6.396 mV/(mg/dL), 0.999, respectively, which is an increase of 50.7% to 111.8% compared to static conditions. The average sensitivity of the urea biosensor to temperature effects is 3.020 mV/(mg/dL) at room temperature, and as the temperature of the solution increases, the average sensitivity of the biosensor also increases, reaching 4.381 mV/(mg/dL) at 37°C and 6.521 mV/(mg/dL) at 45°C, which is an increase of 45.1% to 115.9% compared to room temperature. conditions was 0.19mV/hr, while under dynamic conditions, it was 1.47mV/hr. Although the dynamic measurement values are higher than the static measurement values, the static measurement has more instability factors, while the dynamic measurement maintains a consistent trend. Overall, the measurement results of the urea biosensor under dynamic conditions are superior to those under static conditions, and the dynamic measurement system can be used to mimic the physiological environment of the human body.

ACKNOWLEDGMENT

The authors would like to extend their appreciation to the Taiwan Semiconductor Research Institute (TSRI) for the technical support they most generously extended.

REFERENCES

[1] C. Farmer, E. Fenu, N. O'Flynn, and B. Guthrie, "Clinical assessment and management of multimorbidity: Summary of NICE guidance," *BMJ*, vol. 354, Sep. 2016, Art. no. i4843.
[2] B. M. Brenner, "Hemodynamically mediated glomerular injury and the progressive nature of kidney disease," *Kidney Int.*, vol. 23, no. 4, pp. 647–655, Apr. 1983.

[3] M. Pippias and C. R. V. Tomson, "Patient safety in chronic kidney disease: Time for nephrologists to take action," *Nephrol. Dialysis Transpl.*, vol. 29, no. 3, pp. 473–475, Mar. 2014.
[4] N. Tangri et al., "A predictive model for progression of chronic kidney disease to kidney failure," *J. Amer. Med. Assoc.*, vol. 305, no. 15, pp. 1553–1559, Apr. 2011.
[5] A. S. Levey et al., "Expressing the modification of diet in renal disease study equation for estimating glomerular filtration rate with standardized serum creatinine values," *Clin. Chem.*, vol. 53, no. 4, pp. 766–772, Apr. 2007.
[6] C. Ziegler and W. Göpel, "Biosensor development," *Current Opin. Chem. Biol.*, vol. 2, no. 5, pp. 585–591, Jan. 1998.
[7] J. van der spiegel, I. Lauks, P. Chan, and D. Babic, "The extended gate chemically sensitive field effect transistor as multi-species microprobe," *Sensors Actuators*, vol. 4, pp. 291–298, Jan. 1983.
[8] T. Vo-Dinh and B. Cullum, "Biosensors and biochips: Advances in biological and medical diagnostics," *Fresenius J. Anal. Chem.*, vol. 366, no. 6, pp. 540–551, Mar. 2000.
[9] M. Mascini and S. Tombelli, "Biosensors for biomarkers in medical diagnostics," *Biomarkers*, vol. 13, nos. 7–8, pp. 637–657, Jan. 2008.
[10] C. Griesche and A. J. Baeumner, "Biosensors to support sustainable agriculture and food safety," *TrAC Trends Anal. Chem.*, vol. 128, Jul. 2020, Art. no. 115906.
[11] G. K. Mishra, A. Barfidokht, F. Tehrani, and R. K. Mishra, "Food safety analysis using electrochemical biosensors," *Foods*, vol. 7, no. 9, p. 9, Sep. 2018.
[12] S. Rodriguez-Mozaz, M. J. L. de Alda, M.-P. Marco, and D. Barceló, "Biosensors for environmental monitoring: A global perspective," *Talanta*, vol. 65, no. 2, pp. 291–297, Jan. 2005.
[13] C. I. L. Justino, A. C. Duarte, and T. A. P. Rocha-Santos, "Recent progress in biosensors for environmental monitoring: A review," *Sensors*, vol. 17, no. 12, p. 12, Dec. 2017.
[14] E. K. Sackmann, A. L. Fulton, and D. J. Beebe, "The present and future role of microfluidics in biomedical research," *Nature*, vol. 507, no. 7491, p. 7491, Mar. 2014.
[15] P. S. Dittrich and A. Manz, "Lab-on-a-chip: Microfluidics in drug discovery," *Nat. Rev. Drug Disc.*, vol. 5, no. 3, p. 3, Mar. 2006.
[16] J. El-Ali, P. K. Sorger, and K. F. Jensen, "Cells on chips," *Nature*, vol. 442, p. 7101, Jul. 2006.
[17] A. W. Martinez, S. T. Phillips, G. M. Whitesides, and E. Carrilho, "Diagnostics for the developing world: Microfluidic paper-based analytical devices," *Anal. Chem.*, vol. 82, no. 1, pp. 3–10, Jan. 2010.
[18] G. Xing, W. Zhang, N. Li, Q. Pu, and J.-M. Lin, "Recent progress on microfluidic biosensors for rapid detection of pathogenic bacteria," *Chin. Chem. Lett.*, vol. 33, no. 4, pp. 1743–1751, Apr. 2022.
[19] H. Becker and L. E. Locascio, "Polymer microfluidic devices," *Talanta*, vol. 56, no. 2, pp. 267–287, Feb. 2002.
[20] Y. Zhang et al., "Construction of liquid metal-based soft microfluidic sensors via soft lithography," *J. Nanobiotechnol.*, vol. 20, no. 1, p. 246, May 2022.
[21] D. Erickson and D. Li, "Integrated microfluidic devices," *Analytica Chimica Acta*, vol. 507, no. 1, pp. 11–26, Apr. 2004.
[22] H. Quan, T. Zhang, H. Xu, S. Luo, J. Nie, and X. Zhu, "Photo-curing 3D printing technique and its challenges," *Bioactive Mater.*, vol. 5, no. 1, pp. 110–115, Mar. 2020.
[23] N. Shahrubudin, T. C. Lee, and R. Ramlan, "An overview on 3D printing technology: Technological, materials, and applications," *Procedia Manuf.*, vol. 35, pp. 1286–1296, Jan. 2019.
[24] A. D. Aladese and H.-H. Jeong, "Recent developments in 3D printing of droplet-based microfluidics," *BioChip J.*, vol. 15, no. 4, pp. 313–333, Dec. 2021.
[25] G. D. O'Neil, S. Ahmed, K. Halloran, J. N. Janusz, A. Rodríguez, and I. M. T. Rodríguez, "Single-step fabrication of electrochemical flow cells utilizing multi-material 3D printing," *Electrochem. Commun.*, vol. 99, pp. 56–60, Feb. 2019.
[26] I. Belmonte and R. J. White, "3-D printed microfluidics for rapid prototyping and testing of electrochemical, aptamer-based sensor devices under flow conditions," *Analytica Chimica Acta*, vol. 1192, p. 9, Feb. 2022.
[27] P.-Y. Kuo, T.-H. Wang, W.-H. Lai, and C.-H. Chang, "Analysis and measurements of an urea biosensor based on instrumentation amplifier chip with cross-coupled technique," *IEEE Trans. Instrum. Meas.*, vol. 72, pp. 1–9, 2023.
[28] J.-C. Chou et al., "Novel potentiometric non-enzymatic ascorbic acid sensor based on molybdenum oxide film and copper nanoparticles," *IEEE Sensors J.*, vol. 22, no. 1, pp. 50–60, Jan. 2022.
[29] Y.-F. Bai, T.-B. Xu, J. H. T. Luong, and H.-F. Cui, "Direct electron transfer of glucose oxidase-boron doped diamond interface: A new solution for a classical problem," *Anal. Chem.*, vol. 86, no. 10, pp. 4910–4918, May 2014.
[30] I. Migneault, C. Dartiguenave, M. J. Bertrand, and K. C. Waldron, "Glutaraldehyde: Behavior in aqueous solution, reaction with proteins, and application to enzyme crosslinking," *BioTechniques*, vol. 37, no. 5, pp. 790–802, Nov. 2004.
[31] E. H. Tümer and H. Y. Erbil, "Extrusion-based 3D printing applications of PLA composites: A review," *Coatings*, vol. 11, no. 4, p. 4, Apr. 2021.
[32] G. Velho, P. Froguel, R. Sternberg, D. R. Thevenot, and G. Reach, "*In Vitro* and *In Vivo* stability of electrode potentials in needle-type glucose sensors: Influence of needle material," *Diabetes*, vol. 38, no. 2, pp. 164–171, Feb. 1989.
[33] C.-P. Huang, Y.-K. Li, and T.-M. Chen, "A highly sensitive system for urea detection by using CdSe/ZnS core-shell quantum dots," *Biosensors Bioelectron.*, vol. 22, no. 8, pp. 1835–1838, Mar. 2007.
[34] J.-C. Chou, G.-C. Ye, D.-G. Wu, and C.-C. Chen, "Fabrication of the array chlorine ion sensor based on microfluidic device framework," *Solid-State Electron.*, vol. 77, pp. 87–92, Nov. 2012.
[35] S. Kumar et al., "Microfluidic-integrated biosensors: Prospects for point-of-care diagnostics," *Biotechnol. J.*, vol. 8, no. 11, pp. 1267–1279, Sep. 2013.
[36] G. J. Tangelder, D. W. Slaaf, T. Arts, and R. S. Reneman, "Wall shear rate in arterioles in vivo: least estimates from platelet velocity profiles," *Amer. J. Physiol. Heart Circulatory Physiol.*, vol. 254, no. 6, pp. H1059–H1064, Jun. 1988.
[37] A. R. Pries, T. W. Secomb, and P. Gaehtgens, "The endothelial surface layer," *Eur. J. Physiol.*, vol. 440, no. 5, pp. 653–666, Sep. 2000.
[38] Y. Qin and J. M. S. Cabral, "Kinetic studies of the urease-catalyzed hydrolysis of urea in a buffer-free system," *Appl. Biochem. Biotechnol.*, vol. 49, no. 3, pp. 217–240, Dec. 1994.
[39] S.-Y. Chang, C.-Y. Wang, M.-K. Chen, and C.-E. Li, "Ru incorporation on marked enhancement of diffusion resistance of multi-component alloy barrier layers," *J. Alloys Compd.*, vol. 509, no. 5, pp. L85–L89, Feb. 2011.
[40] B. Krajewska, M. Leszko, and W. Zaborska, "Urease immobilized on chitosan membrane: Preparation and properties," *J. Chem. Technol. Biotechnol.*, vol. 48, no. 3, pp. 337–350, Jun. 1990.
[41] J.-C. Chou et al., "The flexible arrayed non-enzymatic CZO glucose sensor utilizing silver nanowires and nafion," *IEEE Trans. Instrum. Meas.*, vol. 70, pp. 1–11, Jul. 2021.
[42] J.-C. Chou et al., "The characteristic analysis of IGZO/Al pH sensor and glucose biosensor in static and dynamic measurements," *IEEE Sensors J.*, vol. 16, no. 23, pp. 8509–8516, Feb. 2016.
[43] J.-C. Chou et al., "Enzymatic urea sensor based on graphene oxide/titanium dioxide films modified by urease-magnetic beads," *IEEE Trans. Nanotechnol.*, vol. 18, pp. 336–344, Mar. 2019.
[44] J.-C. Chou et al., "The analysis of the urea biosensors using different sensing matrices via wireless measurement system & microfluidic measurement system," *Sensors*, vol. 19, no. 13, p. 13, Jan. 2019.
[45] Y.-H. Nien et al., "Investigation of flexible arrayed urea biosensor based on graphene oxide/nickel oxide films modified by au nanoparticles," *IEEE Trans. Instrum. Meas.*, vol. 70, pp. 1–9, 2020.
[46] B. Öndeş, F. Akpınar, M. Uygun, M. Muti, and D. Aktaş Uygun, "High stability potentiometric urea biosensor based on enzyme attached nanoparticles," *Microchem. J.*, vol. 160, Jan. 2021, Art. no. 105667,